The statistical morphology of Saturn's equatorial energetic neutral atom emission

J. Kinrade[1,*], A. Bader[1,*], S. V. Badman[1], C. Paranicas[2], D. G. Mitchell[2], D. Constable[1], C. S. Arridge[1], S. W. H. Cowley[3], G. Provan[3]

[1]Department of Physics, Lancaster University, Lancaster (UK)
[2]Johns Hopkins University Applied Physics Laboratory, Laurel, MD (USA)
[3]Department of Physics and Astronomy, University of Leicester, Leicester (UK)
[*]These authors contributed equally to this work

Key Points:

- We present a definitive Cassini-era picture of Saturn's global energetic neutral atom morphology using remote sensing imagery.
- Concentric tori of hydrogen and oxygen emissions are most intense at $\sim 7-10$ Saturn radii in the equatorial plane, offset towards the dayside.
- The intensity within 6−12 Saturn radii exhibits clear rotational modulation with north and south magnetic phase systems.

Corresponding author: J. Kinrade, j.kinrade@lancaster.ac.uk

Abstract

Saturn's magnetosphere is an efficient emitter of energetic neutral atoms (ENAs), created through charge exchange of energetic ions with the extended neutral cloud originating from the icy moon Enceladus. We present an analysis using the complete image set captured by Cassini's Ion Neutral Camera (INCA) to characterise Saturn's average ENA morphology. Concentric tori are formed around the planet by oxygen and hydrogen ENAs, with intensity peaks between 7-10 R_S radial distance, with a $\sim$1-2 R_S dayside offset. Nightside intensity is brighter than the dayside, likely the result of enhancements following large-scale plasma injections from the magnetotail, and influence of the noon-midnight electric field. Global intensity is clearly modulated with the near-planetary rotation period. This Cassini-era profile of Saturn's ENA emission advances our understanding of how volcanic moons can influence plasma dynamics in giant magnetospheres and is timely ahead of the planned JUICE mission, which carries the first dedicated ENA detector to Jupiter.

Plain Language Summary

Saturn is engulfed in a cloud of neutral gas originating from ice fissures on the surface of Enceladus. Some particles collide and exchange charge, separating electrons from ions which are guided by Saturn's magnetic field. This way, Saturn's rotating magnetosphere is loaded with mass which is eventually lost into space via ejections of plasma that stretch magnetic field lines to breaking point. Some charged particles in the outer magnetosphere do not escape, but are fired back towards Saturn with field lines as they snap back into place. These energetic ions collide with neutrals, creating energetic neutral atoms (ENA) that were detectable using the INCA camera onboard Cassini. INCA's pictures of Saturn's magnetosphere reveal dynamic regions of plasma flow, important for understanding the entire system. We present an analysis of the complete INCA image set obtained over Cassini's mission, utilizing years of combined exposure to characterise Saturn's average ENA morphology. Rings of ENAs are located at distances between 7-10 R_S, where the interaction between energetic ions and the neutral cloud is largest. We also find ENA variation with Saturn's rotation period, associated with current systems that modulate the plasma sheet every $\sim$ 10 hours.

1 Introduction

Energetic neutral atoms (ENAs) are produced by charge exchange during particle interactions between space plasmas and neutral gas populations. Remote sensing of ENAs was initially developed for probing the terrestrial magnetosphere (Roelof et al., 1985), providing the first such images of Earth's ring current region (Roelof, 1987). Since then, Cassini was the first mission to carry a dedicated ENA detector to another planet - the Ion Neutral Camera (INCA, Krimigis et al., 2004) – which successfully captured ENA emissions from the magnetospheres of Saturn and Jupiter. First detected by Voyager instruments (Kirsch et al., 1981), Saturn's ENAs have been the subject of much study during Cassini's $\sim$ 13 year tour; the extended neutral gas cloud originating from Enceladus makes the Kronian system an efficient emitter of ENAs. Jupiter's ENA torus was observed remotely during a Cassini flyby of the Jovian system (Krimigis et al., 2002; Mauk et al., 2003) while recent studies have identified ENA signatures in particle measurements from the Jupiter Energetic-particle Detector Instrument (JEDI) onboard the Juno orbiter, revealing emissions associated with moons Io and Europa and the planet itself (Mauk, Clark, et al., 2020; Mauk, Allegrini, et al., 2020). A dedicated ENA imager is planned to fly on the JUICE mission that should arrive at Jupiter within the next decade (Grasset et al., 2013). It is therefore timely that we construct the most complete statistical morphology of Saturn's ENA emission, based on all available Cassini INCA imagery.

Throughout the Cassini mission, INCA imagery has helped to reveal the global plasma dynamics throughout Saturn's magnetosphere. The neutral cloud (primarily hydrogen- and oxygen-based) extends out to at least $\sim 40\,\mathrm{R}_S$ (Melin et al., 2009) and is sustained mainly by outgassing from Enceladus, but also the planet's rings and atmosphere. ENA production primarily occurs at radial distances from the outer edge of the E-ring/Rhea's orbit ($\sim 8\,\mathrm{R}_S$) out to Titan's orbit at $\sim 20\,\mathrm{R}_S$ (e.g., Carbary, Mitchell, Brandt, Roelof, & Krimigis, 2008a). Note the inherent dependence on the background neutral distribution means that peak ENA intensities are not necessarily coincident with peak ion intensities. A significant advantage of INCA is the global views of plasma circulation patterns it provides, complementing the partial picture obtained through in situ particle surveys of Voyager (Lazarus & McNutt, 1983) and Cassini (e.g., Sergis et al., 2007; McAndrews et al., 2009; Thomsen et al., 2014; Wilson et al., 2017).

Discrete, rotating regions of enhanced ENA intensity are commonly observed, interpreted as signatures of large-scale plasma injection from the magnetotail (e.g., Mitchell et al., 2005; Mitchell, Krimigis, et al., 2009; Mitchell et al., 2015; Krimigis et al., 2007). Typically appearing around midnight-dawn local times near Titan's orbit, the hot ion population (revealed through ENA detection) drifts around the planet with $\sim 60 - 70\,\%$ of the planetary corotation speed (Carbary, Mitchell, Brandt, Roelof, & Krimigis, 2008b; Carbary & Mitchell, 2014; Kinrade et al., 2020), eventually dispersing through charge exchange. These injection signatures sometimes persist for several planetary rotations (Paranicas et al., 2005), spreading with gradient-curvature drift (e.g., Mitchell, Krimigis, et al., 2009) and often leading to a partial ring or spiral morphology (e.g., Brandt et al., 2008). Re-energization of existing ENA enhancements in the midnight sector can prolong their lifetime (Mitchell, Krimigis, et al., 2009). Kilometric radio (SKR) and ultraviolet auroral signatures have been observed simultaneously with rotating ENA enhancements (e.g., Mitchell, Krimigis, et al., 2009; Lamy et al., 2013; Nichols et al., 2014; Kinrade et al., 2020; Palmaerts et al., 2020; Wing et al., 2020) indicating the presence of a transient field-aligned current system that links injected plasma population sources to the ionosphere; indeed these rotating signatures are a major component of Saturn's auroral emission (Bader et al., 2019). INCA also provides a remote measure of the periodicities known as planetary period oscillations (PPOs) which are present throughout Saturn's magnetosphere (Krimigis et al., 2005; Paranicas et al., 2005; Carbary, Mitchell, Brandt, Paranicas, & Krimigis, 2008; Carbary & Mitchell, 2013), complimenting the other primary indicators of periodicity; namely in situ particle detections (e.g., Clarke et al., 2010; Arridge et al., 2011; Carbary et al., 2017; Ramer et al., 2017), magnetometer (e.g., Andrews et al., 2012, 2019; Provan et al., 2012, 2016) and kilometric radiation measurements (e.g., Desch, 1982; Gurnett et al., 2009; Ye et al., 2016; Lamy, 2017).

Carbary, Mitchell, Brandt, Roelof, and Krimigis (2008a) provided the first statistical maps of Saturn's ENA distribution, using equatorial projections of high latitude ($> 40°$) INCA images captured across 120 days in 2007. Torus-shaped distributions were found in hydrogen and oxygen, largely concentric with the planet and with intensity peaks at distances $\sim$ 8-11 R_S. These long time-based ENA averages are useful for the development of global physical models and boundary information; assimilation and inversion methods can be applied to INCA imagery to reconstruct the global neutral or ion populations (Brandt et al., 2008; Dialynas et al., 2013; Roelof & Skinner, 2000).

In this study we present a statistical analysis of Saturn's ENA distribution using all available Cassini INCA images. We developed an algorithm to ingest and calibrate the raw data and project it into the equatorial plane, detailed in the accompanying technical report by Bader, Kinrade, et al. (2020). Using multi-dimensional histograms we are able to filter observations by pixel-specific parameters carrying information about observation geometry and target location in fixed and rotating reference frames, and create long-term mean averages.

2 Remote sensing ENA imagery

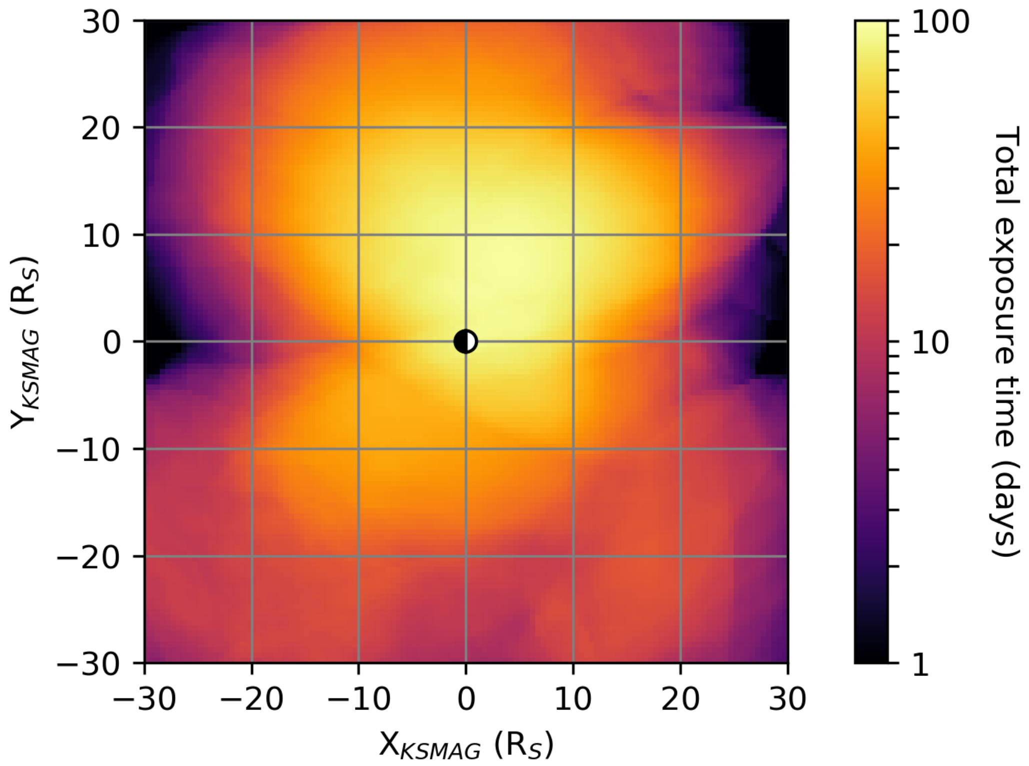

Figure 1. Map of total accumulated exposure time used for this statistical study. This is based on the sample distribution of projected pixels with LOS distance within $30\,R_S$ of the spacecraft and at least 50° inclination angle. Shown is the equatorial plane of Saturn as seen from above the north pole, with the Sun located to the right. While some regions near the edges of the projection have been observed for less than a day, most pixels include tens to hundreds of days of total exposure.

INCA was a time of flight detector on the Cassini orbiter which investigated the Saturn system for more than a decade. It was part of the Magnetosphere IMaging Instrument (MIMI) package whose scientific goals were to study the dynamics and configuration of Saturn's magnetosphere and its interaction with the solar wind and Saturn's moons (Krimigis et al., 2004). Toward these goals INCA was capable of observing either ions or ENAs in keV energy ranges and determining their mass, energy and direction of motion. Its large field of view covering $120° \times 90°$ allowed it to measure significant parts of the ion pitch angle distribution when operated in ion mode (Mitchell, Kurth, et al., 2009; Bader, Badman, et al., 2020), or to perform global observations of ENAs in Saturn's magnetosphere when operated in neutral mode.

Over its 13+ years in orbit around Saturn, ENA observations were obtained from a variety of different perspectives – the resulting dataset of ENA imagery is hence not homogeneous or easy to unify. We countered this difficulty by projecting all observations into Saturn's equatorial plane where most ENAs are created due to increased ion and neutral densities. The processing steps and the newly created dataset are described in more detail in a dedicated technical report by Bader, Kinrade, et al. (2020). Characterisation of the vertical ENA emission structure away from the magnetic/spin equator requires the use of a different projection routine and remains a possibility for future work.

In this study we use the new dataset of ENA projections to obtain long-term averages of the ENA intensity in Saturn's equatorial plane throughout the Cassini mission. This is done by calculating histograms across the entire dataset; we bin the data by spatial location (X/Y_{KSMAG}, radial distance, local time, PPO phase, ...) and by the observed ENA intensity. The ENA intensity binning hereby covers differential ENA fluxes between 10^{-15} and 10^4 particles/cm^2/s/sr/keV in 380 logarithmic bins, resulting in a resolution of 20 bins per order of magnitude. Mean intensities are then calculated using the number of observations in each histogram bin. As described in detail in Bader, Kinrade, et al. (2020), many projections are unsuitable for use as the viewing geometry under which they were obtained leads to pixel stretching or significant loss of resolution. Here we chose to only take into account measurements from spacecraft line-of-sight distances between $5-30\,R_S$ from a given pixel, and from spacecraft elevations between $50-90°$ above a given pixel. Projections showing signs of data contamination (from sunlight or ion leakage in neutral imaging mode) were identified in Bader, Kinrade, et al. (2020) and excluded from this study.

Figure 1 shows the resulting total exposure time across the region of interest within the above constraints. The view is in the Saturn-centered Kronocentric Solar Magnetic (KSMAG) frame, looking down on Saturn from above the north hemisphere with sun direction to the right. This distribution is largely a function of the varying Cassini orbit geometries throughout the mission; some pixel areas were observed for over 100 days in accumulation, with most of the projected coverage within $20\,R_S$ having at least 10 days exposure.

3 Results

3.1 Mean intensity distributions

Figure 2 shows the resulting maps of mean ENA intensity following our processing procedure. As with Figure 1, the view is of the KSMAG equatorial plane, as seen from above the north hemisphere, with the Sun to the right of each image. Panels 2a-b show the hydrogen 24-55 keV and 55-90 keV images, respectively, and panels 2c-d the oxygen 90-170 keV and 170-230 keV images, respectively. Note the logarithmic colour scale mapping, and the shift in scale between 2a-b and 2c-d.

The toroidal morphology is striking in all four cases. This is formed by a region of low-level emission near to the planet within $5\,R_S$ (energetic ions are efficiently absorbed within these distances, e.g., Paranicas et al., 2008), and a ring of enhanced emission beyond this point which varies with energy (see Figure 3). The emissions are near-continuous in local time, with the intensity generally appearing brighter on the nightside than the dayside. A slight dayside offset of the tori by several R_S is also perceptible, with the emission ring several Saturn radii further away from the planet than on the nightside (most clearly in the 24-55 keV hydrogen). The low level emission within $\sim 5\,R_S$ may be attributed to a combination of emission from the planet (e.g., Mitchell, Krimigis, et al., 2009), spreading of observed intensities by the INCA point spread function (Mauk et al., 2003) and the projection procedure.

3.2 Local time - distance profiles

To quantify the morphology further, Figure 3 unwraps the intensity maps of Figure 2 into a local time - distance frame. We have also applied Gaussian fits to each local time bin to determine the radial distance of the ENA intensity peak (black dotted line in each panel). These Gaussian fit parameters are provided in the Supplementary Information. First we see that the hydrogen ENAs peak at slightly larger radial distances ($\sim$10-13 R_S) than the oxygen ENAs ($\sim$7-10 R_S). These peak distance ranges are consistent with the earlier morphology study by Carbary, Mitchell, Brandt, Roelof, and Krimigis (2008a) who analysed INCA imagery from 120 days in 2007 to reveal ENA intensity peaks at $\sim 11\,R_S$ and $\sim 8\,R_S$ for the hydrogen (20-50 keV) and oxygen (64-144 keV), respectively, albeit at slightly different energy ranges to those used here.

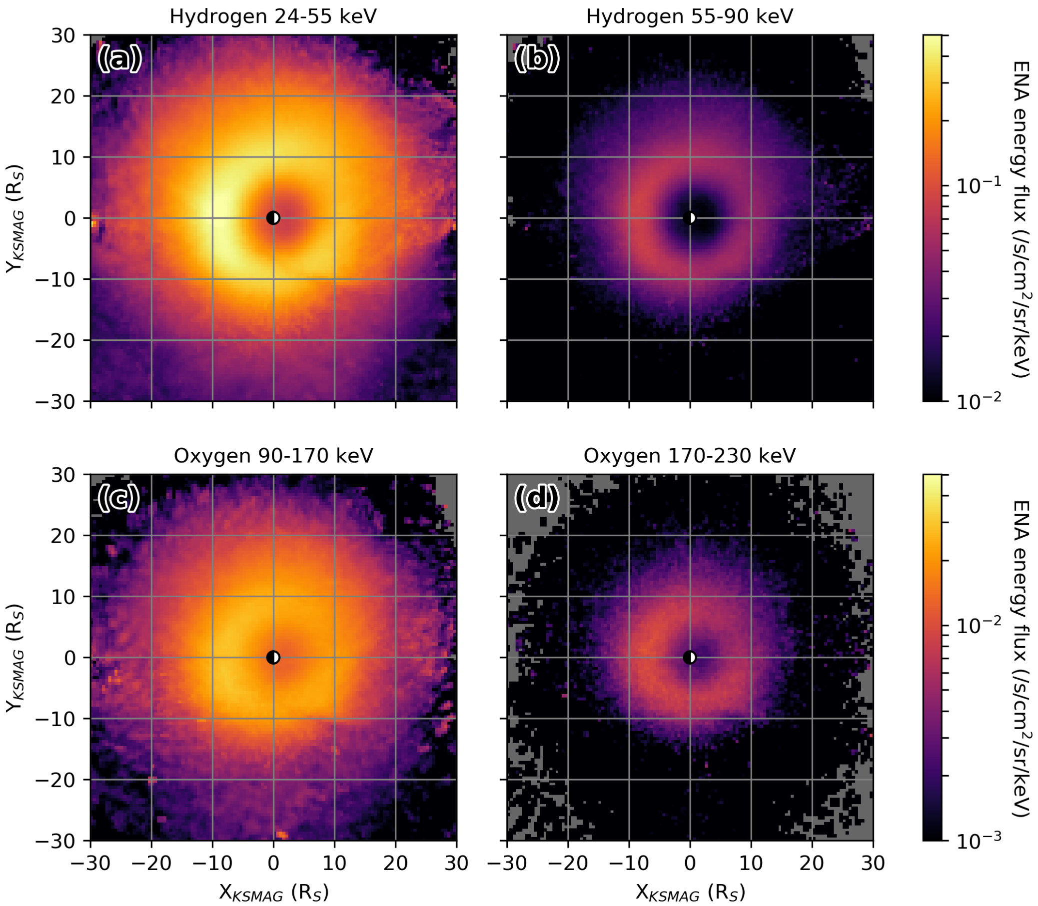

Figure 2. Maps of mean ENA intensities in the equatorial plane of Saturn for each INCA energy band. (a-b) Hydrogen 24-55 keV and 55-90 keV, respectively, and (c-d) oxygen 90-170 keV and 170-230 keV, respectively. The ring shape of the distribution is clear in all cases, with a slight position offset towards the day side and brighter intensities on the night side. Note the logarithmic colour scale mapping, and the shift in scale between (a-b) and (c-d).

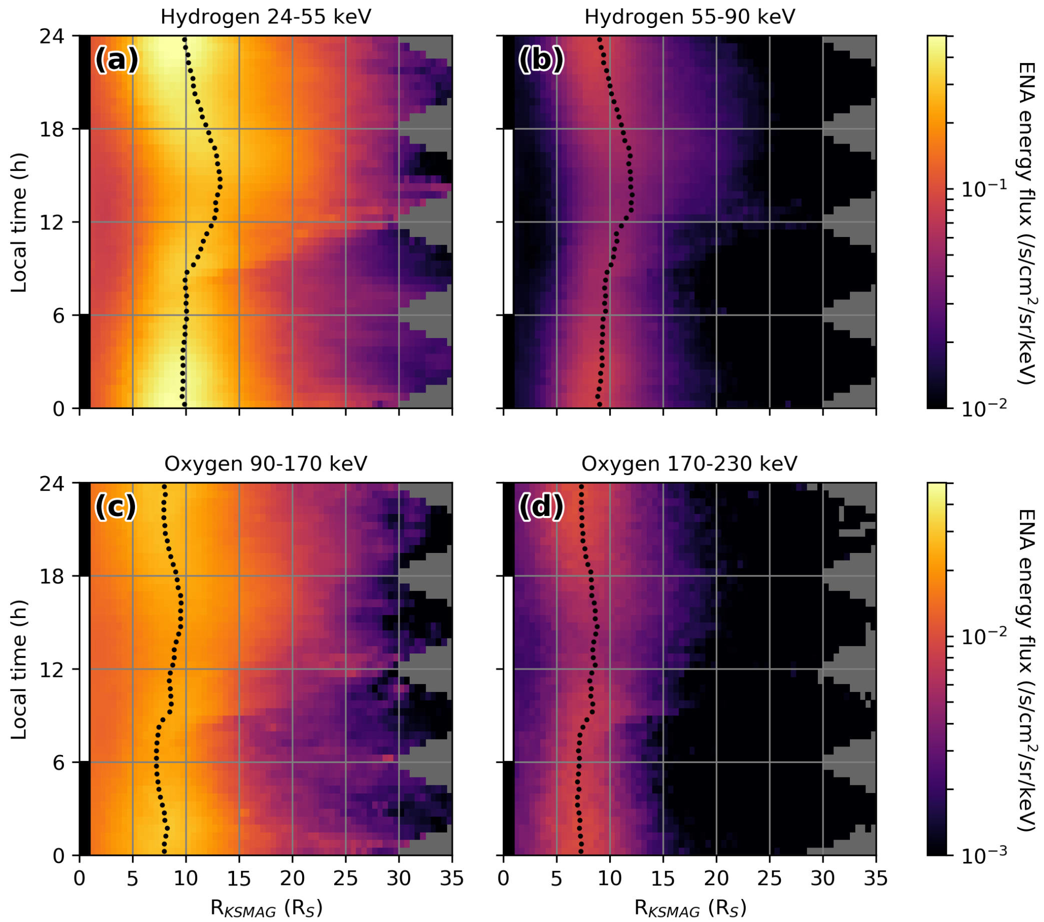

Figure 3. Mean ENA intensity in Saturn's equatorial plane in a local time and radial distance frame. (a-b) Hydrogen 24-55 keV and 55-90 keV, respectively, and (c-d) oxygen 90-170 keV and 170-230 keV, respectively. Note that different color scales apply to (a-b) and (c-d). For each local time bin, the radial intensity profile has been fitted with a Gaussian distribution to determine the radial distance of the ENA intensity peak (black dots).

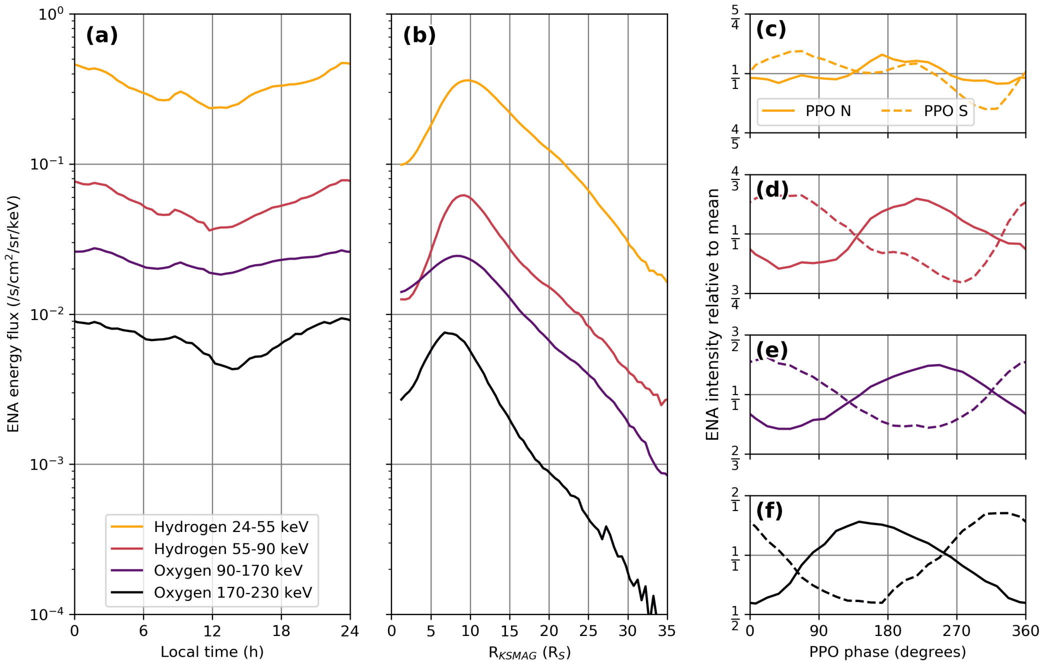

Figure 4. (a) Peak value of the average ENA intensity for each local time bin. (b) Local time-averaged radial ENA intensity profiles. (c-f) Variation of the mean ENA intensity with PPO phase. Shown is the mean ENA intensity at radial distances between 6-12 R_S on Saturn's dayside (6-18 h local time via noon) per PPO bin, relative to the overall mean ENA intensity in this region. Line colors indicate the different particle types and energy ranges as in panels (a-b); solid (dashed) lines indicate the intensity variation with northern (southern) PPO phase.

Second, we observe more clearly here the variation of peak distance with local time, i.e. the dayside offset of the torus apparent in Figure 2. This is clearest in the hydrogen peak fits in images 3a-b, being around $10\,R_S$ on the nightside, but extending to 12-13 R_S on the dayside (post-noon). The offset is less clear in the oxygen distributions. This apparent global shift of the torus towards the dayside could be associated with the fraction of an R_S dawn-dusk trajectory shift of trapped energetic particles which has been associated with the global noon-to-midnight electric field, first discovered by looking at changes in moon wake locations (e.g., Andriopoulou et al., 2012; Thomsen et al., 2012). Wilson et al. (2013), analysing in situ thermal plasma velocity and magnetic field measurements from Cassini, showed that the electric field is actually offset from the noon-midnight meridian by several hours local time, with the dusk-dawn drift velocity imposed on the global plasma circulation in the post-dawn direction out to at least $15\,R_S$ (Wilson et al., 2017). This offset has also been observed in other data sets (e.g., Andriopoulou et al., 2014; Roussos et al., 2019; Sun et al., 2019) and may be produced by variation in the radial force balance at different LTs (Jia & Kivelson, 2016). This may explain why the ENA tori are offset outwards towards post-noon, signifying the point at which particles begin to return inwards again in their displaced orbit. The dawn-dusk asymmetry is evident at distances out to $\sim 30\,R_S$ in the lower energy ENAs, suggesting that the E-field is effective at larger distances than previously considered. The offset appears to be less pronounced on the dayside for the higher energy bands, comparing the hydrogen peak fits in Figure 3a and b. This could be because the higher energy ions are less affected in their trajectory by the electric field asymmetry and thus show smaller orbital displacements, as discussed by (Thomsen et al., 2012).

Average local time and radial distance profiles may be extracted from Figure 3, which is what we show in Figure 4a-b for each imaging energy range. Panel 4a shows the peak value of the average intensity for each local time bin, and panel 4b shows the local-time averaged radial ENA intensity profiles. Note the logarithmic intensity scale in each case. Two general morphological trends are apparent. The ENA intensity is brighter on the nightside than the dayside (by almost half an order of magnitude), and the mean tori distance decreases with species energy (there being a 1-2 R_S shift between the respective hydrogen and oxygen energy peaks in panel 4b). The first of these trends is likely a consequence of periodic injections of energetic plasma from Saturn's nightside following magnetotail reconnection events which disperse as they rotate towards the dayside. The intensity asymmetry is also consistent with the effects of the noon-midnight electric field, as the particle energy and differential flux decrease adiabatically when transported outward on the dayside into regions of lower field strength and lower neutral density. Secondly, the decrease in tori radius with increasing particle energy may be related to the penetration depth of energetic ions and their effective charge exchange cross-section which is a function of energy, i.e. higher energy ions travel further inwards radially to a region of higher neutral density before producing an ENA (e.g., Paranicas et al., 2008). Shifting energetic ions and electrons to low L-shells is considered difficult because of gradient-curvature drift out of the injection flow channels. This result may indicate that the long-term ENA picture we see is dominated by large-scale plasma flows, wider azimuthally than those typically associated with interchange processes. Oxygen ions may also be penetrating the inner magnetosphere at higher charge states (subject to lower gradient-curvature drift), before breaking down to lower charge states and producing ENAs (e.g., Paranicas et al., 2020). Hao et al. (2020) recently showed that the transient noon-midnight electric field can also be responsible for accelerating electrons to the inner magnetosphere, an effect which also extends to energetic ions.

3.3 Planetary period modulation

Periodicity in ENAs was observed early in the Cassini mission (Krimigis et al., 2005), and was first explained by Paranicas et al. (2005) as originating from a rotating point source imposed on a constant, global ring-type emission. Carbary, Mitchell, Brandt, Paranicas, and Krimigis (2008) then quantified the modulation periods in a Lomb-Scargle analysis of dawn-dusk ENA intensity variation using imagery taken from low-latitudes between 2004-2007. They found that 64-144 keV oxygen ENAs exhibited strong periodicity around 10.8 hours, i.e. near planetary-period (specifically the period of southern PPO system which was dominant at that time), while the 20-50 keV hydrogen periodicity varied between 8-13 hours. We know from keogram track analysis of high-latitude imagery that most rotating ENA enhancements move with speeds around 60-70% corotation (e.g., Carbary, Mitchell, Brandt, Roelof, & Krimigis, 2008b; Carbary & Mitchell, 2014; Kinrade et al., 2020), which may explain the wider range of periodicities observed in the hydrogen emission. So how can we test for the near planetary-period modulation of global ENA emissions?

Any rotational modulation of the mean global ENA intensity should result from the interaction of both north and south PPO current systems as they superpose in the magnetic equator. The main effect of this interaction (in addition to north-south current sheet displacement) is modulation of the plasma sheet thickness, as the perturbation field vector periodically reinforces and weakens the core field depending on phases and relative strengths of the northern and southern systems (e.g., Provan et al., 2012; Cowley et al., 2017; Thomsen et al., 2017; Bradley et al., 2018, 2020). This effect acts to minimize the thickness of the plasma sheet at PPO longitudes $\Psi_N = 0°$ and $\Psi_S = 180°$, when reconnection in the tail (and therefore, possibly, subsequent ENA intensification following injections) is statistically more likely to occur (Jackman et al., 2016; Bradley et al., 2018). Conversely, a thicker plasma sheet would intuitively lead to more ions interacting with the neutrals to produce more ENAs. Such variations in the electron density (i.e. thick and dense vs thin and tenuous) have been observed by the Cassini Langmuir Probe (Morooka et al., 2009). The thickness modulation is amplified when the north-south PPO systems superpose in antiphase, and is reduced when the systems rotate in phase relative to one another.

Here we order all projected INCA pixels by their corresponding magnetic phase to reveal any periodicity present in the global ENA intensity. For a given exposure time, each pixel has a magnetic longitude with respect to both the northern and southern PPO phases, and throughout the Cassini mission the N-S phase systems swept through various periods of beat configuration and relative strengths. In Figure 4c-f we show the relative ENA intensities at each energy band within the main toroid region of 6-12 R_S on Saturn's dayside (6-18 h local time), as a fraction of the mean intensity, versus the north and south magnetic phase. We chose to only investigate dayside observations to remove noisy intensity fluctuations arising from magnetotail dynamics. Note also that local time dependence is lost when binning the pixels with respect to the rotating phase systems.

The sinusoidal response visible in all panels of Figure 4c-f indicates that the ENA intensities within the main toroid distances are being modulated within the frame of the rotating phase systems. The modulation is strongest in the 170-230 keV oxygen emission (4f), the intensity varying periodically between almost double ($\sim 140°$ N, $\sim 315°$ S) and half ($\sim 5°$ N, $\sim 175°$ S) the mean level for both phase systems. The 55-90 keV hydrogen (4d) and 90-170 keV oxygen (4e) emission responses also show clear modulation, but with a slight shift in phasing compared to higher energy oxygen. The 90-170 keV oxygen peaks at a northern phase of $\sim 225°$, for example, compared to $\sim 140°$ for the higher energy band. This higher energy phase shift is in the right direction for gradient-curvature spread of the ions to be a contributing factor, but the magnitude of the shift ($\sim 90°$) seems too large for the energy difference here alone. The radial phase delay across these distances is only minor ($\sim 30°$ from 9-15 R_S, Andrews et al., 2010) such that we do not expect a strong smoothing effect from averaging across the 6-12 R_S radial range. If we consider that the ENA intensifications may result from a more distant energisation and injection process then it would be appropriate to consider the retarded phase at which they originated (e.g., Bradley et al., 2018). Such an investigation is beyond the scope of the current study. The key finding is the anti-phase nature of these responses in the north and south rotating frames, indicating that the global ENA production is affected at some level by changes in plasma sheet thickness and density driven by the rotating perturbation fields as described above. The phases where the intensity peaks occur are all around $\sim 180°$ N, $\sim 0°$ S, indicating maximum ENA emission from the thicker, more dense plasma sheet sector. We are unable to explain here why the strength of the rotational modulation on the ENA intensity increases with energy, but this is an interesting result that warrants further study.

4 Conclusions

We have analysed high-latitude Cassini INCA images of Saturn's equatorial ENA emission, using data from the entire mission. The result is the definitive Cassini-era picture of Saturn's equatorial ENA morphology obtained through remote sensing. The emissions are observed across four imaging bands; low and high energy hydrogen-derived ENAs (24-55 keV and 55-90 keV, respectively), and low and high energy oxygen (90-170 keV and 170-230 keV, respectively). We have used a new algorithm to sort, calibrate and project this ENA imagery into the equatorial plane for analysis, documented in Bader, Kinrade, et al. (2020). The final processed images are based on up to hundreds of days of accumulative exposure in some regions of the magnetosphere.

The long time average structure of the ENA emission is a torus around the planet, with intensity peaks at distances between 7-10 R_S (the hydrogen emission peaking $\sim 1-2\,R_S$ further away from Saturn than the oxygen). This is consistent with both the inner boundary of the high particle pressure region between 8-14 R_S (e.g., Sergis et al., 2007) and where the total neutral density starts to ramp up towards the inner magnetosphere within $\sim 8\,R_S$ (e.g., Cassidy & Johnson, 2010). The neutrals peak around 4 Rs near Enceladus' orbit (e.g., Richardson et al., 1998; Dialynas et al., 2013), whereas inward-travelling energetic particles of up to several hundred keV start to drop in number around L-shells of 8-9 (Paranicas et al., 2008), so the ENAs are reflecting the ion population and not just the neutral density profile. ENA intensity is generally higher on the nightside than the dayside by almost half an order of magnitude, likely the result of persistent, large-scale plasma injection activity manifesting in these long-time average pictures, and the conservation of adiabatic invariants as plasma drifts around to the dayside. Another trend common to both species and energy ranges is the radial offset of the torus towards post-noon local times by up to $3\,R_S$, which may be at least partly attributable to the trajectory shift experienced by trapped energetic particles under the influence of the global E-field asymmetry.

Rotational modulation of the ENA emission is clearly present within the main tori distances (6-12 R_S), given the sinusoidal pattern of mean intensity variation with both north and south magnetic phases. The 170-230 keV oxygen ENAs exhibit the strongest modulation, varying periodically between almost double and half the mean emission level. This modulation effect decreases continuously with energy, being weakest in the 24-55 keV hydrogen, for reasons yet to be explained. The phase pattern is broadly consistent across all species/energies, and indicates that periodic modulation of the plasma sheet thickness could be driving these variations in ENA production - a thicker plasma sheet would intuitively lead to higher numbers of energetic ions interacting with the neutrals to produce more ENAs.

A fall-off in projection coverage at distances around 15-20 R_S (see Figure 2) - where the main field aligned currents associated with the PPOs are thought to close in the equatorial plane (Andrews et al., 2019) - prevents us from making a robust test of the ENA intensities further out in the magnetosphere. The main ENA tori peak at distances around the possible plasmapause-like boundary identified by (Thomsen et al., 2015), a possible radial limit for injected hot plasma reaching the cooler, denser plasma of the inner magnetosphere. It may be that the modulation we observe here is driven by the combined effects of both plasma sheet thickness variation plus asymmetries in radial plasma flow associated with convection patterns in the inner magnetosphere, such as those identified in electron densities by Gurnett et al. (2007).

Characterising Saturn's ENA distribution is useful for the development and constraint of chemistry models, and advances our understanding of how tiny volcanic moons can ultimately influence so much of the plasma dynamics in giant magnetospheres. This is particularly timely ahead of the planned JUICE explorer mission to Jupiter, which will fly with the first dedicated ENA detector to investigate the Jovian magnetosphere. Aside from being a proxy for ion loss processes, ENA imagery can be reverse-engineered to simulate the background neutral population. A question yet to be fully answered is how rotating ENA enhancements relate to counterpart auroral emissions, and what is the nature of the transient current system linking them during injection activity? Future work should investigate further the nature of the periodicity apparent in the global ENA intensity, how this relates to large-scale plasma injection dynamics, and if this is linked to magnetotail reconnection signatures observed preferentially at certain magnetic perturbation phases.

Acknowledgments

Cassini operations are supported by NASA (managed by the Jet Propulsion Laboratory) and the European Space Agency (ESA). All Cassini INCA data used in this study are available on NASA's Planetary Data System (PDS) (`https://pds.jpl.nasa.gov/`), and we extend our thanks to all members of the Cassini MIMI team for their hard work. INCA ENA projections generated in this study are accessible on the Lancaster University data repository (`http://www.research.lancs.ac.uk/portal/en/datasets/cassini-inca-equatorial-ena-projections(e9cd8998-75ab-4fff-8e6a-9bebb74ab54b).html`). PPO phase data (2004–2017) can be found on the University of Leicester Research Archive (`http://hdl.handle.net/2381/42436`). JK, SVB and DAC were supported by STFC grant ST/R000816/1. SVB was also supported by an STFC Ernest Rutherford Fellowship ST/M005534/1. AB was funded by a Lancaster University FST studentship. CP would like to acknowledge grant NNX16AI46G between NASA and the Johns Hopkins University. CSA was supported by a Royal Society Research Fellowship (UF110442) and STFC grant ST/R000816/1. Work at Leicester by SWHC and GP was supported by STFC Consolidated Grant ST/N000749/1. Computations for this study were performed using the High End Computing facility at Lancaster University.

References

Andrews, D. J., Cowley, S. W., Provan, G., Hunt, G. J., Hadid, L. Z., Morooka, M. W., & Wahlund, J. E. (2019). The Structure of Planetary Period Oscillations in Saturn's Equatorial Magnetosphere: Results From the Cassini Mission. *Journal of Geophysical Research: Space Physics*, *124* (11), 8361–8395. Retrieved from `https://agupubs.onlinelibrary.wiley.com/doi/epdf/10.1029/2019JA026804` doi: 10.1029/2019JA026804

Andrews, D. J., Cowley, S. W. H., Dougherty, M. K., Lamy, L., Provan, G., & Southwood, D. J. (2012). Planetary period oscillations in Saturn's magnetosphere: Evolution of magnetic oscillation properties from southern summer to post-equinox. *Journal of Geophysical Research: Space Physics*, *117* (4). Retrieved from `http://onlinelibrary.wiley.com/doi/10.1029/2011JA017444/abstract` doi: 10.1029/2011JA017444

Andrews, D. J., Cowley, S. W. H., Dougherty, M. K., & Provan, G. (2010). Magnetic field oscillations near the planetary period in Saturn's equatorial magnetosphere: Variation of amplitude and phase with radial distance and local time. *Journal of Geophysical Research: Space Physics*, *115* (A04212), 1–28. Retrieved from `http://onlinelibrary.wiley.com/doi/10.1029/2009JA014729/abstract` doi: 10.1029/2009JA014729

Andriopoulou, M., Roussos, E., Krupp, N., Paranicas, C., Thomsen, M., Krimigis, S., ... Glassmeier, K. H. (2012). A noon-to-midnight electric field and nightside dynamics in Saturn's inner magnetosphere, using microsignature observations. *Icarus*, *220*(2), 503–513. Retrieved from `http://dx.doi.org/10.1016/j.icarus.2012.05.010` doi: 10.1016/j.icarus.2012.05.010

Andriopoulou, M., Roussos, E., Krupp, N., Paranicas, C., Thomsen, M., Krimigis, S., ... Glassmeier, K. H. (2014). Spatial and temporal dependence of the convective electric field in Saturn's inner magnetosphere. *Icarus*, *229*, 57–70. Retrieved from `https://www.sciencedirect.com/science/article/pii/S0019103513004570` doi: 10.1016/j.icarus.2013.10.028

Arridge, C. S., André, N., Khurana, K. K., Russell, C. T., Cowley, S. W. H., Provan, G., ... Young, D. T. (2011). Periodic motion of Saturn's nightside plasma sheet. *Journal of Geophysical Research: Space Physics*, *116*(A11205), 1–22. Retrieved from `http://onlinelibrary.wiley.com/doi/10.1029/2011JA016827/abstract` doi: 10.1029/2011JA016827

Bader, A., Badman, S. V., Cowley, S. W., Yao, Z. H., Ray, L. C., Kinrade, J., ... Pryor, W. R. (2019). The Dynamics of Saturn's Main Aurorae. *Geophysical Research Letters*, *46*(17-18), 10283–10294. Retrieved from `https://agupubs.onlinelibrary.wiley.com/doi/full/10.1029/2019GL084620` doi: 10.1029/2019GL084620

Bader, A., Badman, S. V., Ray, L. C., Paranicas, C. P., Lorch, C. T. S., Clark, G., ... Pryor, W. (2020). Energetic Particle Signatures Above Saturn's Aurorae. *Journal of Geophysical Research: Space Physics*, *125*(1), e2019JA027403. Retrieved from `https://agupubs.onlinelibrary.wiley.com/doi/full/10.1029/2019JA027403#` doi: 10.1029/2019ja027403

Bader, A., Kinrade, J., Badman, S. V. B., Paranicas, C., Constable, D. A., & Mitchell, D. G. (2020). A complete dataset of equatorial projections of Saturn's energetic neutral atom emissions observed by Cassini-INCA. *in preparation*.

Bradley, T. J., Cowley, S. W., Bunce, E. J., Melin, H., Provan, G., Nichols, J. D., ... Hunt, G. J. (2020). Saturn's Nightside Dynamics During Cassini's F Ring and Proximal Orbits: Response to Solar Wind and Planetary Period Oscillation Modulations. *Journal of Geophysical Research: Space Physics*, *125*(9), 1–39. Retrieved from `https://agupubs.onlinelibrary.wiley.com/doi/full/10.1029/2020JA027907` doi: 10.1029/2020JA027907

Bradley, T. J., Cowley, S. W. H., Bunce, E. J., Smith, A. W., Jackman, C. M., & Provan, G. (2018). Planetary Period Modulation of Reconnection Bursts in Saturn's Magnetotail. *Journal of Geophysical Research: Space Physics*, *123*(11), 9476–9507. Retrieved from `https://onlinelibrary.wiley.com/doi/abs/10.1029/2018JA025932` doi: 10.1029/2018JA025932

Brandt, P. C., Paranicas, C. P., Carbary, J. F., Mitchell, D. G., Mauk, B. H., & Krimigis, S. M. (2008). Understanding the global evolution of Saturn's ring current. *Geophysical Research Letters*, *35*(17), 1–5. Retrieved from `http://onlinelibrary.wiley.com/doi/10.1029/2008GL034969/full#footer-citing` doi: 10.1029/2008GL034969

Carbary, J. F., & Mitchell, D. G. (2013). Periodicities in Saturn's Magnetosphere. *Reviews of Geophysics*, *51*, 1–30. Retrieved from `http://onlinelibrary.wiley.com/doi/10.1002/rog.20006/abstract` doi: doi:10.1002/rog.20006

Carbary, J. F., & Mitchell, D. G. (2014). Keogram analysis of ENA images at Saturn. *Journal of Geophysical Research: Space Physics*, *119*, 1771–1780. Retrieved from `http://onlinelibrary.wiley.com/doi/10.1002/2014JA019784/full#references` doi: 10.1002/2014JA020465.Received

Carbary, J. F., Mitchell, D. G., Brandt, P., Paranicas, C., & Krimigis, S. M. (2008). ENA periodicities at Saturn. *Geophysical Research Letters*, *35*(7), 1–5. Retrieved from http://onlinelibrary.wiley.com/doi/10.1029/2008GL033230/full#references doi: 10.1029/2008GL033230

Carbary, J. F., Mitchell, D. G., Brandt, P., Roelof, E. C., & Krimigis, S. M. (2008a). Statistical morphology of ENA emissions at Saturn. *Journal of Geophysical Research: Space Physics*, *113*(5), 1–9. Retrieved from http://onlinelibrary.wiley.com/doi/10.1029/2007JA012873/epdf doi: 10.1029/2007JA012873

Carbary, J. F., Mitchell, D. G., Brandt, P., Roelof, E. C., & Krimigis, S. M. (2008b). Track analysis of energetic neutral atom blobs at Saturn. *Journal of Geophysical Research: Space Physics*, *113*(1), 1–7. Retrieved from https://agupubs.onlinelibrary.wiley.com/doi/full/10.1029/2007JA012708 doi: 10.1029/2007JA012708

Carbary, J. F., Mitchell, D. G., Kollman, P., Krupp, N., & Roussos, E. (2017). Energetic Electron Periodicities during the Cassini Grand Finale. *Journal of Geophysical Research: Space Physics*, *122*. Retrieved from http://onlinelibrary.wiley.com/doi/10.1002/2017JA024836/full doi: 10.1002/2017JA024836

Cassidy, T. A., & Johnson, R. E. (2010). Collisional spreading of Enceladus' neutral cloud. *Icarus*, *209*(2), 696–703. Retrieved from https://www.sciencedirect.com/science/article/pii/S0019103510001582#! doi: 10.1016/j.icarus.2010.04.010

Clarke, K. E., Andrews, D. J., Arridge, C. S., Coates, A. J., & Cowley, S. W. H. (2010). Magnetopause oscillations near the planetary period at Saturn: Occurrence, phase, and amplitude. *Journal of Geophysical Research: Space Physics*, *115*(A08209). Retrieved from https://agupubs.onlinelibrary.wiley.com/doi/full/10.1029/2009JA014745 doi: 10.1029/2009JA014745

Cowley, S. W. H., Provan, G., Hunt, G. J., & Jackman, C. M. (2017). Planetary period modulations of Saturn's magnetotail current sheet: A simple illustrative model. *Journal of Geophysical Research: Space Physics*, *122*, 258–279. Retrieved from http://onlinelibrary.wiley.com/doi/10.1002/2016JA023367/full doi: 10.1002/2017JA023993

Desch, M. D. (1982). Evidence for solar wind control of saturn radio emission. *Journal of Geophysical Research*, *87*(A6), 4549–4554. Retrieved from http://onlinelibrary.wiley.com/doi/10.1029/JA087iA06p04549/full doi: 10.1029/JA087iA06p04549

Dialynas, K., Rymer, A. M., Mitchell, D. G., Hamilton, D. C., Krupp, N., Krimigis, S. M., & Brandt, P. C. (2013). The extended Saturnian neutral cloud as revealed by global ENA simulations using Cassini/MIMI measurements. *Journal of Geophysical Research: Space Physics*, *118*(6), 3027–3041. Retrieved from https://agupubs.onlinelibrary.wiley.com/doi/full/10.1002/jgra.50295 doi: 10.1002/jgra.50295

Grasset, O., Dougherty, M. K., Coustenis, A., Bunce, E. J., Erd, C., Titov, D., … Van Hoolst, T. (2013). JUpiter ICy moons Explorer (JUICE): An ESA mission to orbit Ganymede and to characterise the Jupiter system. *Planetary and Space Science*, *78*, 1–21. Retrieved from http://dx.doi.org/10.1016/j.pss.2012.12.002 doi: 10.1016/j.pss.2012.12.002

Gurnett, D. A., Lecacheux, A., Kurth, W. S., Persoon, A. M., Groene, J. B., Lamy, L., … Carbary, J. F. (2009). Discovery of a north-south asymmetry in Saturn's radio rotation period. *Geophysical Research Letters*, *36*(16), 2–5. Retrieved from http://onlinelibrary.wiley.com/doi/10.1029/2009GL039621/full doi: 10.1029/2009GL039621

Gurnett, D. A., Persoon, A. M., Kurth, W. S., Groene, J. B., Averkamp, T. F., Dougherty, M. K., & Southwood, D. J. (2007). The variable rotation period of the inner region of Saturn's plasma disk. *Science*, *316*(5823), 442–445. Retrieved from https://science.sciencemag.org/content/316/5823/442 doi: 10.1126/science.1138562

Hao, Y.-X., Sun, Y.-X., Roussos, E., Liu, Y., Kollmann, P., Yuan, C.-J., ... Zong, Q.-G. (2020). The Formation of Saturn's and Jupiter's Electron Radiation Belts by Magnetospheric Electric Fields. *The Astrophysical Journal*, *905*(1), L10. Retrieved from http://dx.doi.org/10.3847/2041-8213/abca3fhttps://iopscience.iop.org/article/10.3847/2041-8213/abca3f/meta?casa_token=MjFtr9ZINh4AAAAA:aCYgQjmmmH__ptcrUuVfjR43wSXFXQBcA0k78_58h4OVbbYKHhvaSGPoC_-qv3F-Ea46TRr1DbA doi: 10.3847/2041-8213/abca3f

Jackman, C. M., Provan, G., & Cowley, S. W. H. (2016). Reconnection events in Saturn's magnetotail: Dependence of plasmoid occurrence on planetary period oscillation phase. *Journal of Geophysical Research A: Space Physics*, *121*(4), 2922–2934. Retrieved from https://agupubs.onlinelibrary.wiley.com/doi/full/10.1002/2015JA021985 doi: 10.1002/2015JA021985

Jia, X., & Kivelson, M. G. (2016, feb). Dawn-dusk asymmetries in rotating magnetospheres: Lessons from modeling Saturn. *Journal of Geophysical Research: Space Physics*, *121*(2), 1413–1424. Retrieved from https://onlinelibrary.wiley.com/doi/abs/10.1002/2015JA021950 doi: 10.1002/2015JA021950

Kinrade, J., Badman, S. V., Paranicas, C., Mitchell, D. G., Arridge, C. S., Gray, R. L., ... Achilleos, N. (2020). Tracking Counterpart Signatures in Saturn's Auroras and ENA Imagery During Large-Scale Plasma Injection Events. *Journal of Geophysical Research: Space Physics*, *125*, e2019JA027542. Retrieved from https://agupubs.onlinelibrary.wiley.com/doi/full/10.1029/2019JA027542 doi: 10.1029/2019JA027542

Kirsch, E., Krimigis, S. M., Ip, W. H., & Gloeckler, G. (1981). X-ray and energetic neutral particle emission from Saturn's magnetosphere. *Nature*, *292*(5825), 718–721. Retrieved from https://www.nature.com/articles/292718a0 doi: 10.1038/292718a0

Krimigis, S. M., Mitchell, D. G., Hamilton, D. C., Dandouras, J., Armstrong, T. P., Bolton, S. J., ... Williams, D. J. (2002). A nebula of gases from Io surrounding Jupiter. *Nature*, *415*(6875), 994–996. Retrieved from https://www.nature.com/articles/415994a doi: 10.1038/415994a

Krimigis, S. M., Mitchell, D. G., Hamilton, D. C., Krupp, N., Livi, S., Roelof, E. C., ... Woch, J. (2005). Dynamics of Saturn's magnetosphere from MIMI during Cassini's orbital insertion. *Science*, *307*(5713), 1270–1273. Retrieved from http://www.sciencemag.org/content/307/5713/1270.long doi: 10.1126/science.1105978

Krimigis, S. M., Mitchell, D. G., Hamilton, D. C., Livi, S., Dandouras, J., Jaskulek, S., ... Williams, D. J. (2004). Magnetosphere Imaging Instrument (MIMI) on the Cassini mission to Saturn/Titan. *Space Science Reviews*, *114*(1-4), 233–329. doi: 10.1007/s11214-004-1410-8

Krimigis, S. M., Sergis, N., Mitchell, D. G., Hamilton, D. C., & Krupp, N. (2007). A dynamic, rotating ring current around Saturn. *Nature*, *450*(7172), 1050–1053. Retrieved from https://www.nature.com/articles/nature06425 doi: 10.1038/nature06425

Lamy, L. (2017). The Saturnian Kilometric Radiation before the Cassini Grand Finale. In *Proceedings of the 8th international workshop on planetary, solar and heliospheric radio emissions (pre viii).* Seggauberg, Austria. Retrieved from http://arxiv.org/abs/1709.07693

Lamy, L., Prangé, R., Pryor, W., Gustin, J., Badman, S. V., Melin, H., ... Brandt, P. C. (2013). Multispectral simultaneous diagnosis of Saturn's aurorae throughout a planetary rotation. *Journal of Geophysical Research: Space Physics*, *118*(8), 4817–4843. Retrieved from http://onlinelibrary.wiley.com/doi/10.1002/jgra.50404/abstract doi: 10.1002/jgra.50404

Lazarus, A. J., & McNutt, R. L. (1983). Low-Energy Plasma Ion Observations in Saturn's Magnetosphere. *Journal of Geophysical Research*, *88*(A11), 8831–8846. Retrieved from https://agupubs.onlinelibrary.wiley.com/doi/abs/10.1029/JA088iA11p08831 doi: 10.1029/JA088iA11p08831

Mauk, B. H., Allegrini, F., Bagenal, F., Bolton, S. J., Clark, G., Connerney, J. E., ... Rymer, A. M. (2020). Energetic Neutral Atoms From Jupiter's Polar Regions. *Journal of Geophysical Research: Space Physics*, *125*(12), 1–15. Retrieved from https://agupubs.onlinelibrary.wiley.com/doi/full/10.1029/2020JA028697?saml_referrer doi: 10.1029/2020JA028697

Mauk, B. H., Clark, G., Allegrini, F., Bagenal, F., Bolton, S. J., Connerney, J. E., ... Rymer, A. M. (2020). Juno Energetic Neutral Atom (ENA) Remote Measurements of Magnetospheric Injection Dynamics in Jupiter's Io Torus Regions. *Journal of Geophysical Research: Space Physics*, *125*(5), 1–15. Retrieved from https://agupubs.onlinelibrary.wiley.com/doi/epdf/10.1029/2020JA027964 doi: 10.1029/2020JA027964

Mauk, B. H., Mitchell, D. G., Krimigis, S. M., Roelof, E. C., & Paranicas, C. P. (2003). Energetic neutral atoms from a trans-Europa gas torus at Jupiter. *Nature*, *421*(6926), 920–922. Retrieved from https://www.nature.com/articles/nature01431 doi: 10.1038/nature01431

McAndrews, H. J., Thomsen, M. F., Arridge, C. S., Jackman, C. M., Wilson, R. J., Henderson, M. G., ... Dougherty, M. K. (2009). Plasma in Saturn's nightside magnetosphere and the implications for global circulation. *Planetary and Space Science*, *57*(14-15), 1714–1722. Retrieved from https://www.sciencedirect.com/science/article/pii/S0032063309000750#bib19 doi: 10.1016/j.pss.2009.03.003

Melin, H., Shemansky, D. E., & Liu, X. (2009). The distribution of atomic hydrogen and oxygen in the magnetosphere of Saturn. *Planetary and Space Science*, *57*(14-15), 1743–1753. Retrieved from http://dx.doi.org/10.1016/j.pss.2009.04.014 doi: 10.1016/j.pss.2009.04.014

Mitchell, D. G., Brandt, P. C., Carbary, J. F., Kurth, W. S., Krimigis, S. M., Paranicas, C., ... Pryor, W. R. (2015). Injection, Interchange, and Reconnection: Energetic Particle Observations in Saturn's Magnetosphere. In A. Keiling, C. M. Jackman, & P. A. Delamere (Eds.), *Magnetotails in the solar system* (chap. 19). Hoboken, NJ: John Wiley and Sons, Inc. Retrieved from http://onlinelibrary.wiley.com/doi/10.1002/9781118842324.ch19/summary doi: 10.1002/9781118842324.ch19

Mitchell, D. G., Brandt, P. C., Roelof, E. C., Dandouras, J., Krimigis, S. M., Mauk, B. H., ... Shemansky, D. E. (2005). Energetic ion acceleration in Saturn's magnetotail: Substorms at Saturn? *Geophysical Research Letters*, *32*(20), 1–4. Retrieved from https://agupubs.onlinelibrary.wiley.com/doi/full/10.1029/2005GL022647 doi: 10.1029/2005GL022647

Mitchell, D. G., Krimigis, S. M., Paranicas, C., Brandt, P. C., Carbary, J. F., Roelof, E. C., ... Pryor, W. R. (2009). Recurrent energization of plasma in the midnight-to-dawn quadrant of Saturn's magnetosphere, and its relationship to auroral UV and radio emissions. *Planetary and Space Science*, *57*(14-15), 1732–1742. Retrieved from http://www.sciencedirect.com/science/article/pii/S0032063309001044 doi: 10.1016/j.pss.2009.04.002

Mitchell, D. G., Kurth, W. S., Hospodarsky, G. B., Krupp, N., Saur, J., Mauk, B. H., ... Hamilton, D. C. (2009). Ion conics and electron beams associated with auroral processes on Saturn. *Journal of Geophysical Research: Space Physics*, *114*(A02212). Retrieved from https://agupubs.onlinelibrary.wiley.com/doi/full/10.1029/2008JA013621 doi: 10.1029/2008ja013621

Morooka, M. W., Modolo, R., Wahlund, J. E., André, M., Eriksson, A. I., Persoon, A. M., ... Dougherty, M. (2009). The electron density of Saturn's magnetosphere. *Annales Geophysicae*, *27*(7), 2971–2991. Retrieved from https://angeo.copernicus.org/articles/27/2971/2009/ doi:

10.5194/angeo-27-2971-2009

Nichols, J. D., V.badman, S., Baines, K. H., Brown, R. H., Bunce, E. J., Clarke, J. T., ... Stallard, T. S. (2014). Dynamic auroral storms on Saturn as observed by the Hubble Space Telescope. *Geophysical Research Letters*, *41*(10), 3323–3330. Retrieved from http://onlinelibrary.wiley.com/doi/10.1002/2014GL060186/abstract doi: 10.1002/2014GL060186

Palmaerts, B., Yao, Z. H., Sergis, N., Guo, R. L., Grodent, D., Dialynas, K., ... Mitchell, D. G. (2020). A Long-Lasting Auroral Spiral Rotating Around Saturn's Pole. *Geophysical Research Letters*, *47*(23), 1–10. Retrieved from https://agupubs.onlinelibrary.wiley.com/doi/full/10.1029/2020GL088810?casa_token=7kvj3ezuX3YAAAAA%3AqGC-a4RIoN4-P2S-Pb6DlDFqyzrV1bL7eeiwG-sDyPf-A3dVsZT_Kp4YBmhFX9C3Rq7yay6Eoh8eT5JXSg doi: 10.1029/2020GL088810

Paranicas, C., Mitchell, D. G., Krimigis, S. M., Hamilton, D. C., Roussos, E., Krupp, N., ... Armstrong, T. P. (2008). Sources and losses of energetic protons in Saturn's magnetosphere. *Icarus*, *197*(2), 519–525. Retrieved from https://www.sciencedirect.com/science/article/pii/S0019103508002133 doi: 10.1016/j.icarus.2008.05.011

Paranicas, C., Mitchell, D. G., Roelof, E. C., Brandt, P. C., Williams, D. J., Krimigis, S. M., & Mauk, B. H. (2005). Periodic intensity variations in global ENA images of Saturn. *Geophysical Research Letters*, *32*(21), 1–4. Retrieved from http://onlinelibrary.wiley.com/doi/10.1029/2005GL023656/full doi: 10.1029/2005GL023656

Paranicas, C., Thomsen, M. F., Kollmann, P., Azari, A. R., Bader, A., Badman, S. V., ... Roussos, E. (2020). Inflow Speed Analysis of Interchange Injections in Saturn's Magnetosphere. *Journal of Geophysical Research: Space Physics*, *125*(9), e2020JA028299. Retrieved from https://agupubs.onlinelibrary.wiley.com/doi/10.1029/2020JA028299 doi: 10.1029/2020JA028299

Provan, G., Andrews, D. J., Arridge, C. S., Coates, a. J., Cowley, S. W. H., Cox, G., ... Jackman, C. M. (2012). Dual periodicities in planetary-period magnetic field oscillations in Saturn's tail. *Journal of Geophysical Research: Space Physics*, *117*(1), 1–20. Retrieved from http://onlinelibrary.wiley.com/doi/10.1029/2011JA017104/abstract doi: 10.1029/2011JA017104

Provan, G., Cowley, S. W. H., Lamy, L., Bunce, E. J., Hunt, G. J., Zarka, P., & Dougherty, M. K. (2016). Planetary period oscillations in Saturn's magnetosphere: Coalescence and reversal of northern and southern periods in late northern spring. *Journal of Geophysical Research: Space Physics*, *121*, 9829–9862. Retrieved from http://onlinelibrary.wiley.com/doi/10.1002/2016JA023056/full doi: 10.1002/2016JA023056

Ramer, K. M., Kivelson, M. G., Sergis, N., Khurana, K. K., & Jia, X. (2017). Spinning, breathing, and flapping: Periodicities in Saturn's middle magnetosphere. *Journal of Geophysical Research: Space Physics*, *122*(1), 393–416. Retrieved from https://agupubs.onlinelibrary.wiley.com/doi/full/10.1002/2016JA023126 doi: 10.1002/2016JA023126

Richardson, J. D., Eviatar, A., McGrath, M. A., & Vasyliūnas, V. M. (1998, aug). OH in Saturn's magnetosphere: Observations and implications. *Journal of Geophysical Research: Planets*, *103*(E9), 20245–20255. Retrieved from http://doi.wiley.com/10.1029/98JE01127 doi: 10.1029/98JE01127

Roelof, E. C. (1987, jun). Energetic neutral atom image of a storm-time ring current. *Geophysical Research Letters*, *14*(6), 652–655. Retrieved from https://agupubs.onlinelibrary.wiley.com/doi/abs/10.1029/GL014i006p00652http://doi.wiley.com/10.1029/GL014i006p00652 doi: 10.1029/GL014i006p00652

Roelof, E. C., Mitchell, D. G., & Williams, D. J. (1985). Energetic neutral atoms (E

∼ 50 keV) from the ring current: IMP 7/8 and ISEE 1. *Journal of Geophysical Research*, *90*(A11), 10991. Retrieved from http://doi.wiley.com/10.1029/JA090iA11p10991 doi: 10.1029/JA090iA11p10991

Roelof, E. C., & Skinner, A. J. (2000). Extraction of ion distributions from magnetospheric ENA and EUV images. *Space Sci. Rev.*, *91*(1-2), 437–459. Retrieved from https://link.springer.com/article/10.1023/A:1005281424449 doi: 10.1023/A:1005281424449

Roussos, E., Kollmann, P., Krupp, N., Paranicas, C., Dialynas, K., Jones, G. H., ... Cooper, J. F. (2019). Sources, Sinks, and Transport of Energetic Electrons Near Saturn's Main Rings. *Geophysical Research Letters*, *46*(7), 3590–3598. Retrieved from https://agupubs.onlinelibrary.wiley.com/doi/full/10.1029/2018GL078097 doi: 10.1029/2018GL078097

Sergis, N., Krimigis, S. M., Mitchell, D. G., Hamilton, D. C., Krupp, N., Mauk, B. M., ... Dougherty, M. (2007). Ring current at Saturn: Energetic particle pressure in Saturn's equatorial magnetosphere measured with Cassini/MIMI. *Geophysical Research Letters*, *34*(9), 1–6. Retrieved from http://onlinelibrary.wiley.com/doi/10.1029/2006GL029223/full doi: 10.1029/2006GL029223

Sun, Y. X., Roussos, E., Krupp, N., Zong, Q. G., Kollmann, P., & Zhou, X. Z. (2019). Spectral Signatures of Adiabatic Electron Acceleration at Saturn Through Corotation Drift Cancelation. *Geophysical Research Letters*, *46*(17-18), 10240–10249. Retrieved from https://agupubs.onlinelibrary.wiley.com/doi/full/10.1029/2019GL084113?casa_token=lkBOPhr7xPkAAAAA%3AL6NJsFyw6ceo6Lg_wYjKNvpk_tzn5cu5LZH1nDTq3gbapTDND3jjZgZEBVyxtXPrhwTMdvdIFbfxF-cSLw doi: 10.1029/2019GL084113

Thomsen, M. F., Jackman, C. M., Cowley, S. W., Jia, X., Kivelson, M. G., & Provan, G. (2017). Evidence for periodic variations in the thickness of Saturn's nightside plasma sheet. *Journal of Geophysical Research: Space Physics*, *122*(1), 280–292. Retrieved from http://onlinelibrary.wiley.com/doi/10.1002/2016JA023368/full doi: 10.1002/2016JA023368

Thomsen, M. F., Jackman, C. M., Tokar, R. L., & Wilson, R. J. (2014). Plasma flows in Saturn's nightside magnetosphere. *Journal of Geophysical Research: Space Physics*, *119*, 4521–4535. Retrieved from http://onlinelibrary.wiley.com/doi/10.1002/2014JA019912/abstract doi: 10.1002/2014JA019912

Thomsen, M. F., Mitchell, D. G., Jia, X., Jackman, C. M., Hospodarsky, G., & Coates, A. J. (2015). Plasmapause formation at Saturn. *Journal of Geophysical Research: Space Physics*, *120*, 2571–2583. Retrieved from http://onlinelibrary.wiley.com/doi/10.1002/2015JA021008/abstract doi: 10.1002/2015JA021008

Thomsen, M. F., Roussos, E., Andriopoulou, M., Kollmann, P., Arridg, C. S., Paranicas, C. P., ... Young, D. T. (2012). Saturn's inner magnetospheric convection pattern: Further evidence. *Journal of Geophysical Research: Space Physics*, *117*(9), 1–19. Retrieved from https://agupubs.onlinelibrary.wiley.com/doi/full/10.1029/2011JA017482 doi: 10.1029/2011JA017482

Wilson, R. J., Bagenal, F., Delamere, P. A., Desroche, M., Fleshman, B. L., & Dols, V. (2013). Evidence from radial velocity measurements of a global electric field in Saturn's inner magnetosphere. *Journal of Geophysical Research: Space Physics*, *118*(5), 2122–2132. Retrieved from https://agupubs.onlinelibrary.wiley.com/doi/10.1002/jgra.50251 doi: 10.1002/jgra.50251

Wilson, R. J., Bagenal, F., & Persoon, A. M. (2017). Survey of thermal plasma ions in Saturn's magnetosphere utilizing a forward model. *Journal of Geophysical Research: Space Physics*, *122*(7), 7256–7278. Retrieved from https://agupubs.onlinelibrary.wiley.com/doi/full/10.1002/2017JA024117 doi:

10.1002/2017JA024117

Wing, S., Brandt, P. C., Mitchell, D. G., Johnson, J. R., Kurth, W. S., & Menietti, J. D. (2020). Periodic Narrowband Radio Wave Emissions and Inward Plasma Transport at Saturn's Magnetosphere. *The Astronomical Journal*, *159*(6), 249. Retrieved from `https://iopscience.iop.org/article/10.3847/1538-3881/ab818d/pdf` doi: 10.3847/1538-3881/ab818d

Ye, S. Y., Fischer, G., Kurth, W. S., Menietti, J. D., & Gurnett, D. A. (2016). Rotational modulation of Saturn's radio emissions after equinox. *Journal of Geophysical Research: Space Physics*, *121*. Retrieved from `http://onlinelibrary.wiley.com/doi/10.1002/2016JA023281/full` doi: 10.1002/2016JA023281